

Genesis and evolution of extended defects: The role of evolving interface instabilities in cubic SiC

Cite as: Appl. Phys. Rev. **7**, 021402 (2020); doi: 10.1063/1.5132300

Submitted: 17 October 2019 · Accepted: 16 March 2020 ·

Published Online: 28 April 2020



View Online



Export Citation



CrossMark

Giuseppe Fisicaro,^{1,a)} Corrado Bongiorno,¹ Ioannis Deretzis,¹ Filippo Giannazzo,¹ Francesco La Via,¹ Fabrizio Roccaforte,¹ Marcin Zielinski,² Massimo Zimbone,³ and Antonino La Magna^{1,b)}

AFFILIATIONS

¹Consiglio Nazionale delle Ricerche, Istituto per la Microelettronica e Microsistemi (CNR-IMM), Z.I. VIII Strada 5, I-95121 Catania, Italy

²NOVASIC, Savoie Technolac, Arche Bat 4, BP267, 73375 Le Bourget du Lac, France

³Consiglio Nazionale delle Ricerche, Istituto per la Microelettronica e Microsistemi (CNR-IMM), V. S. Sofia 64, 95129 Catania, Italy

^{a)}Author to whom correspondence should be addressed: Giuseppe.Fisicaro@imm.cnr.it

^{b)}Electronic mail: Antonino.Lamagna@imm.cnr.it

ABSTRACT

Emerging wide bandgap semiconductor devices such as the ones built with SiC have the potential to revolutionize the power electronics industry through faster switching speeds, lower losses, and higher blocking voltages, which are superior to standard silicon-based devices. The current epitaxial technology enables more controllable and less defective large area substrate growth for the hexagonal polymorph of SiC (4H-SiC) with respect to the cubic counterpart (3C-SiC). However, the cubic polymorph exhibits superior physical properties in comparison to its hexagonal counterpart, such as a narrower bandgap (2.3 eV), possibility to be grown on a silicon substrate, a reduced density of states at the SiC/SiO₂ interface, and a higher channel mobility, characteristics that are ideal for its incorporation in metal oxide semiconductor field effect transistors. The most critical issue that hinders the use of 3C-SiC for electronic devices is the high number of defects in bulk and epilayers, respectively. Their origin and evolution are not understood in the literature to date. In this manuscript, we combine *ab initio* calibrated Kinetic Monte Carlo calculations with transmission electron microscopy characterization to evaluate the evolution of extended defects in 3C-SiC. Our study pinpoints the atomistic mechanisms responsible for extended defect generation and evolution, and establishes that the antiphase boundary is the critical source of other extended defects such as single stacking faults with different symmetries and sequences. This paper showcases that the eventual reduction of these antiphase boundaries is particularly important to achieve good quality crystals, which can then be incorporated in electronic devices.

© 2020 Author(s). All article content, except where otherwise noted, is licensed under a Creative Commons Attribution (CC BY) license (<http://creativecommons.org/licenses/by/4.0/>). <https://doi.org/10.1063/1.5132300>

I. INTRODUCTION

The growth of high-quality substrates for microelectronic applications is one of the key elements that drive society toward a more sustainable green economy. The development of new high-power and high-current devices for clean energy production, energy harvesting, and energy conversion is a crucial asset for limiting the use of carbon-based fuels. Decreasing the size and weight of power devices would be very desirable, as well as reducing their cooling requirements while maintaining their high performances at elevated temperatures.

Emerging wide bandgap semiconductor devices, like those built with silicon carbide (SiC), can revolutionize power electronics through faster switching speeds, lower losses, and higher blocking voltages, with respect to standard silicon-based devices.^{1–4} Its physical properties allow operation in harsh environments and high temperatures, yielding increased power density with reduced thermal management

requirements, while avoiding expensive heat sinks at the device scale. Although the current epitaxial technology enables more controllable and less defective substrates for the hexagonal polymorph of SiC (4H-SiC) with respect to the cubic polytype (3C-SiC),⁵ the latter is the only one that can be grown on a silicon substrate, leading to a significant reduction of the growth cost. Furthermore, the relatively narrow bandgap of 3C-SiC (2.3 eV) with respect to 4H-SiC (3.28 eV) results in a reduced density of states at the SiO₂/3C-SiC interface, allowing for a higher channel mobility of >300 cm²/(V · s) for Metal Oxide Semiconductor Field Effect Transistors (MOSFETs). Such mobility values have not been achieved for any other SiC polytype.^{6,7} This aspect implies a remarkable reduction in the power consumption of these switching devices, with an important reduction of overall CO₂ emission. A further advantage of 3C-SiC compared to 4H-SiC is the much lower temperature coefficient of resistance between room

temperature and 200 °C, which leads to a large reduction of device-on-resistance at realistic junction temperatures for power device operation.

The growth and fabrication of high-quality 3C-SiC epilayers and bulk wafers is becoming very important.^{8,9} The most crucial issue that hinders the use of 3C-SiC is the high number of defects in both bulk and epilayers. Therefore, an intense research effort has been dedicated to this problem.^{5,10–13}

With this respect, as in the synthesis process of any material, the interplay between surface instabilities that occur during the crystal growth, bulk defects, and crystal boundaries are key issues for the understanding of the kinetics involved in the growth process.^{5,14–17} Indeed, morphological and micro-structural characterizations of grown crystals often indicate a clear correlation between the defective structures and the evolution of the interfaces during the synthesis stage.^{1,18–20} Silicon carbide crystals are a test bed for these studies due to the extreme polymorphism caused by the small energetic cost of stacking disorder. The different sequences of SiC bi-layers in the three symmetric positions (conventionally named ABC) of the hexagonal close packing creates more than 250 different polytypes (polytype instability).^{21–23} A direct consequence of the huge polymorphic character of SiC is the facile generation of extended defects in a plethora of configurations. The Stacking Faults (SFs) class is probably the most common and most studied one, due to the tight relationship with the SiC polytypism. In addition, crystallography studies often focus on antiphase boundaries (APBs), micropipes, dislocations, and other kinds of missing crystal homogeneity.^{1,24}

Knowledge on defects in 3C-SiC crystals is usually obtained by post-growth experimental characterizations. However, the genesis and the evolution of crystal imperfections is, in the majority of cases, a moving interface/surface. As a consequence, due to the lack of reliable *in situ* dynamic analyses of the evolving systems, it is difficult to achieve the correct and complete description of the atomic mechanisms governing this complex phenomenology. The integration of structural analysis and process simulations could overcome these difficulties.^{25–34} However, it is easy to understand that the simulation tools should achieve the following unconventional performances: (a) A structural evolution occurring on macroscopic time scales (from seconds to hours); and (b) a simulation mechanism that can be correctly modeled only at the atomic scale, as a result of the cooperative dynamics of (at least) billions of atoms.

Several theoretical approaches have been suggested to study the SiC crystal growth, which can be categorized as off-lattice approaches (*ab initio*,^{35,36} molecular dynamics,³⁷ and related structure optimization procedures^{38,39}) or on-lattice [e.g., Kinetic Lattice Monte Carlo (KLMC)].⁴⁰ Off-lattice codes with continuous particle positions can be used for the research of defects but are unable to reach the time scales of the epitaxial process. The latter can be hindered either by the full simulation with lattice vibrations or by the evaluation of the relevant barriers from the potential energy surface on the fly.

Stochastic simulations within the KLMC approach^{41–45} could satisfy the two requirements of atomic accuracy and large-scale simulations, allowing for a multi-scale description of the epitaxial growth process. On-lattice models (including Lattice Gas and Solid-on-Solid approaches) are characterized by evolving Monte Carlo particles that lay on the perfect lattice sites but fail in correctly describing the generation and evolution of extended defects.^{42,46,47}

In particular, previous KLMC methods formulated for silicon carbide materials suffer from fundamental limitations: they either allow approximate defect simulation but do not simulate separately the evolution of the two system atoms, i.e., Si and C, in the compound,^{29,48} or they simulate Si and C individually, but the defect formation and evolution cannot be estimated.^{40,49,50}

A Kinetic Monte Carlo (KMC) formulation on augmented or superlattices offers great flexibility to simulate the structural evolution of defective systems, overcoming all previously noted limits. We simulate the complex kinetics scenario^{1,5,24,51} during growths of cubic SiC by means of a recently developed stochastic Kinetic Monte Carlo superLattice (KMCsL) code,⁵² which aims at simulating with an atomistic resolution the growth process of compound materials characterized by sp^3 bond symmetry. The peculiar characteristic of this method is the possibility to study the generation and evolution of extended and point defects during the growth process. In particular, in the class of extended defects, stacking faults and APBs are of primary interest due to their impact on the material quality and their negative consequences when building devices and applications. The code treats carbon and silicon atoms as independent particles. In order to increase the predictive power of the KMCsL simulations, we make use of *ab initio* calculations at a density functional theory level to extract the energetics needed to set rate constants within the Transition State Theory for the active Monte Carlo particles.

We combine *ab initio* calculations of several surface configurations and the temperature dependence of the solid/vapor SiC-phase equilibrium to specifically calibrate the event rates for 3C-SiC. The analysis of several equivalent replicas of the KMCsL evolution starting from the same initial defective seed [reproducing a 3C-SiC crystal with two different (anti)phase domains] discloses a variety of kinetic behaviors, which finds a clear counterpart in real growth processes, revealing the atomic mechanisms responsible for extended defect generation and evolution.

II. EXPERIMENTAL

The growth process was performed using a Chemical Vapor Deposition (CVD) reactor, on (001) “on axis” oriented Si substrates, using silane (SiH_4), propane (C_3H_8), and H_2 as silicon precursor, carbon precursor, and gas carrier, respectively.^{53,54} A multi-step growth process was carried out: it comprises “etching,” “carbonization,” “growth,” and “cooling down” steps. Each of these steps consists of further sub steps. Etching was performed under an H_2 flux at a temperature of 1100 °C. During carbonization, the temperature was set to 1120 °C, and propane was added to the carrier gas. The growth was performed at 1300 °C with both Si and C precursors. The growth rates were maintained at 1 $\mu m/h$. Finally, the temperature was decreased until reaching room temperature, and the chamber was flushed with Ar in order to avoid etching of the surface due to the presence of hydrogen.

Focused samples were characterized by means of High Angle Annular Dark Field Scanning Transmission Electron Microscopy (HAADF-STEM) and conductive atomic force microscopy (CAFM). HAADF-STEM was carried out on a Cs-corrected JEOL ARM200F probe, equipped with a cold field emission gun and working at 200 kV. We operated with three detectors, having a low, medium, and very high scattering angle, respectively. The dark field detector inner semi-angle (80 mrad) allowed the signal to be roughly proportional to the atomic number Z .⁵⁵ Under these conditions the intensities observed in the scanning transmission electron microscopy micrographs could be

directly interpreted. The microscope has a nominal resolution of 0.68 Å.

Nanoscale resolution current mapping and morphological images of the 3C-SiC layers grown on the Si (001) substrate were obtained by CAFM.^{56–58} These analyses were carried out using the TUNA module of the DI-3100 microscope with the Nanoscope V controller. The current maps were acquired with a Pt coated Si tip scanned on the sample surface, by applying a DC bias between this conductive tip and a macroscopic Ni₂Si Ohmic contact fabricated onto 3C-SiC. In this configuration, local inhomogeneities in the conductivity of 3C-SiC associated with electrically active defects reaching the sample surface can be directly visualized.

III. COMPUTATIONAL

Crystal growth was simulated by means of a KMCsL approach, designed to study at an atomic resolution the growth kinetics of elements, alloys, and compounds characterized by the sp³ bond symmetry. Formalization and implementation details of the KMCsL code are discussed in Ref. 52. Deposition and evaporation are the active Monte Carlo events, driving the stochastic evolution. In the application of the KMCsL to the SiC material presented here, the silicon and carbon atoms undergo independent kinetics. We point out and demonstrate in the following that a dense superlattice, where the original lattice of the ideal crystal is a sublattice of the superlattice itself, can correctly accommodate a large class of SiC defective configurations.^{27,48,52} Indeed, the code is able to simulate the evolution of both point-like and extended defects, like stacking faults of different symmetries, APBs, and grain boundaries. Moreover, the KMCsL can also simulate the morphology evolution during the growth (e.g., the epitaxial growth or etching of flat, structured, or patterned substrates, as well as nanoparticles of various shapes). In the case of surfaces, periodic boundary conditions are applied in the planes that are orthogonal to the growth direction.

In order to be reliably applied to a given material, configuration-dependent parameters in KMCsL have to be calibrated using a more fundamental approach, or by means of a fitting procedure with *ad hoc* experiments performed in controlled conditions. Following a sequential multiscale approach, we used *ab initio* energetics at a density functional theory level to set temperature-dependent input frequencies for the local transitions involving atoms bonded X ∈ {C, Si} to the evolving SiC surface/interfaces (i.e., the subset of under-coordinated atoms at a given time *t* of the simulation⁵²). As such transitions imply bond breaking, we assume that the related KMCsL evaporation frequencies follow Arrhenius-type functions of the generalized binding energies $E\{\Sigma_{loc}(X, t)\}$ for the X detachment,

$$\nu(X, t) = \nu_0(T) \times \exp\left[\frac{-E\{\Sigma_{loc}(X, t)\}}{kT}\right]. \quad (1)$$

We note that the frequency in Eq. (1) depends on the local atomic configurations $\Sigma_{loc}(X, t)$ around atom X before the transition, which we classify in the current KMCsL approximation by means of the number (one/two/three) of sp³ X-Si and X-C bonds in the first-neighbor shell (see Sec. S1 of the [supplementary material](#) for the setting of the evaporation energetics and frequencies). Arrhenius pre-factors $\nu_0(T)$ have been set with partial pressures at equilibrium in the gas phase during silicon carbide sublimation.⁵⁹ We notice that in the absence of deposition, the method is also calibrated to the

temperature-dependent sublimation kinetics of the SiC material in equilibrium with its gas components.

Deposition frequencies depend on the experimental controlled growth conditions implemented in the CVD^{60–63} or physical vapor deposition^{1,64} chambers. In our modeling approach, these frequencies are again configuration dependent. They reproduce the average rate of

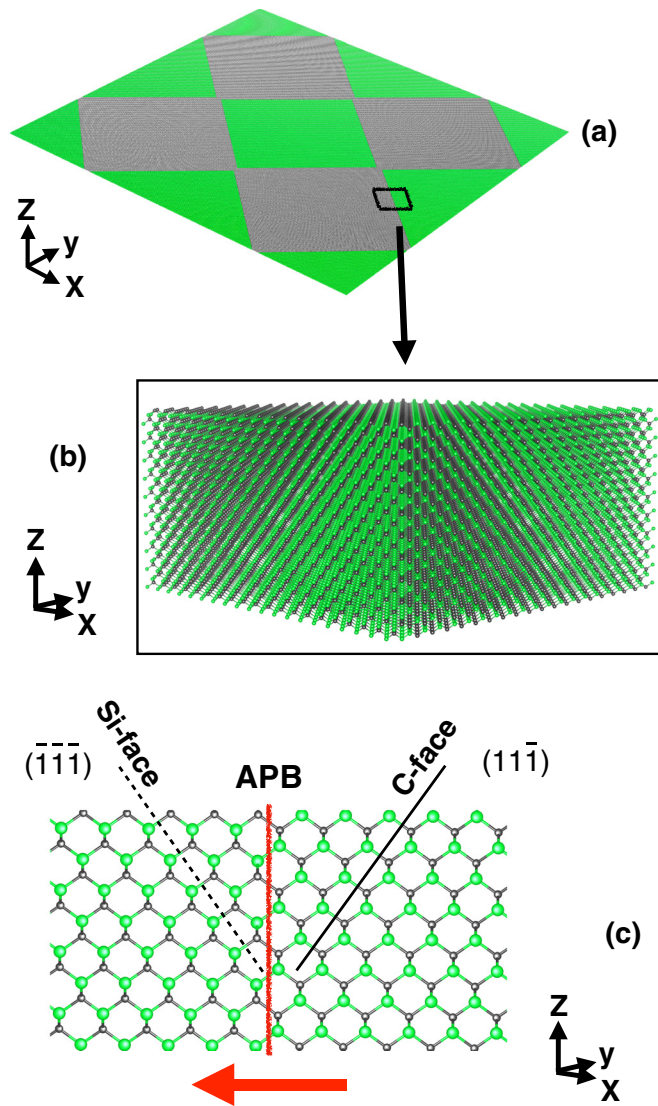


FIG. 1. (a) Scheme of antiphase domains made from the periodic replicas in the xy plane of the initial simulation domain [shown in Fig. 2(b)]. Green (silicon) and gray (carbon) atoms outline the four APB and the different polarities of the substrate: considering the periodic boundary conditions on the xy plane, the substrate looks like an outline of APDs, favoring defect interactions in a reasonable time and space scale. (b) Zoom of the antiphase boundary with anti-sites along {110} crystal planes; (c) orthogonal view of an antiphase boundary (110), representing a zoom of the APB shown in the (b) panel. The dashed and continuous segments highlight, respectively, the (111) Si-face and the (111) C-face with different polarities; the red arrow depicts the APB drift during an epitaxial growth along the (001) surface due to the different growth velocity of the exposed (111) C-face and the (111) Si-face.

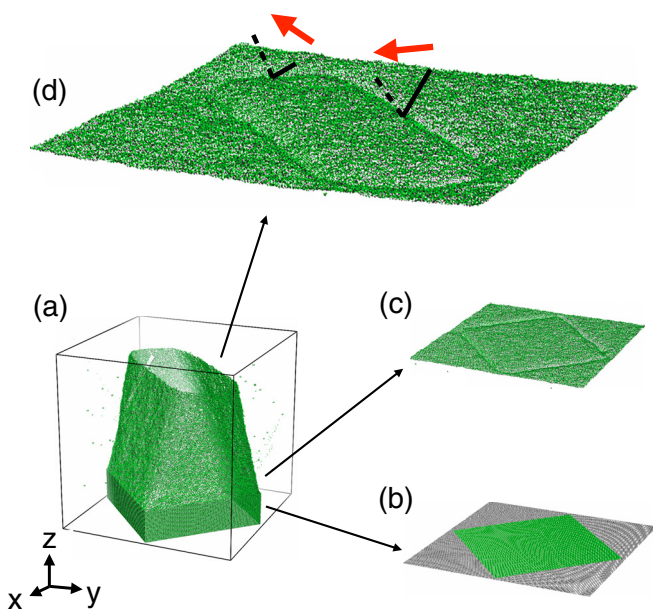


FIG. 2. Evolution of an APD with four APBs along the $\{110\}$ planes during the 3C-SiC substrate growth along the [001] z direction. Epitaxially grown 3C-SiC substrate: (a) atoms at the antiphase boundaries in the bulk; (b) under-coordinated atoms of the input KMC substrate, highlighting the initial xy surface exposed to the deposited gases; (c) under-coordinated atoms taken after the start of the KMC deposition, highlighting the formation of the surface depletion at the APB; and (d) under-coordinated atoms taken at the end of the KMC evolution, highlighting the final xy surface. The dashed and continuous segments highlight, respectively, the $\{111\}$ Si-face and C-face; the red arrow depicts the APB drift during an epitaxial growth due to the different growth velocity of the exposed $\{111\}$ Si-face and C-face.

the Si or C atoms attached/released at the solid surface independently from the particular reactions' mechanisms involving atomic or molecular components in the vapor phase. We have calibrated these parameters in order to reproduce experimental time-dependent SiC profiles in CVD growth processes on structured silicon substrates with

inverted pyramid patterns,^{53,54} grown with the same method described in Sec. II. The simulated evolution starts from a SiC seed, reproducing the growth step only (for the calibration of the KMCsL deposition frequencies see Sec. S1 of the [supplementary material](#)). In our case, KMCsL deposition parameters guarantee, as in the experimental case,⁶¹ controlled simulated epitaxial growth with a low generation of point defects (vacancies or anti-sites). The generation flux rate of point defects is below $2.0 \times 10^{10} \text{ cm}^{-2} \text{ s}^{-1}$, while bulk annihilation events are not considered here, since we focus our analysis on the evolution of extended defects.

We simulated the epitaxial growth of 3C-SiC substrates exposing the (001) surface (the z axis of the Cartesian system lies along the [001] direction). A cubic simulation box with a side of 740.8 \AA was set. Considering the superlattice description, the box contained $\sim 8 \times 10^9$ sites. We started the KMCsL run from a 3C-SiC slab with a thickness of 137.8 \AA . The initial active KMC particles lying at the (001) surface consisted of 51 200 under-coordinated atoms.

The simulation results starting from an ideal 3C-SiC slab (i.e., no defects are considered in the bulk of the initial substrate) with the surface aligned to a (001) plane are discussed in Sec. S2 of the [supplementary material](#). Here we notice that in many replicas of equivalent simulated growths (from the stochastic point of view), no generation of extended defects has been observed, demonstrating that this growth direction is rather robust against extended defect formation. Contrarily, in the absence of a step-flow growth mode, stacking faults form due the polytype instability implemented in the KMCsL model in the case of growth over $\{111\}$ facets.⁵²

In order to evaluate the conduction properties of stacking faults and APBs, we performed quantum transport calculations within the nonequilibrium Green's function formalism,⁶⁵ considering electronic Hamiltonians obtained from the density functional theory (e.g., see Ref. 66). We used the SIESTA code⁶⁷ along with the local density approximation⁶⁸ for the exchange-correlation functional. Electronic wave functions were constructed on a double- ζ polarized basis set for both Si and C, whereas the ionic cores were described with norm-conserving Troullier-Martins pseudopotentials.⁶⁹ All atoms were allowed to fully relax until forces were less than $0.04 \text{ eV}/\text{\AA}$. The

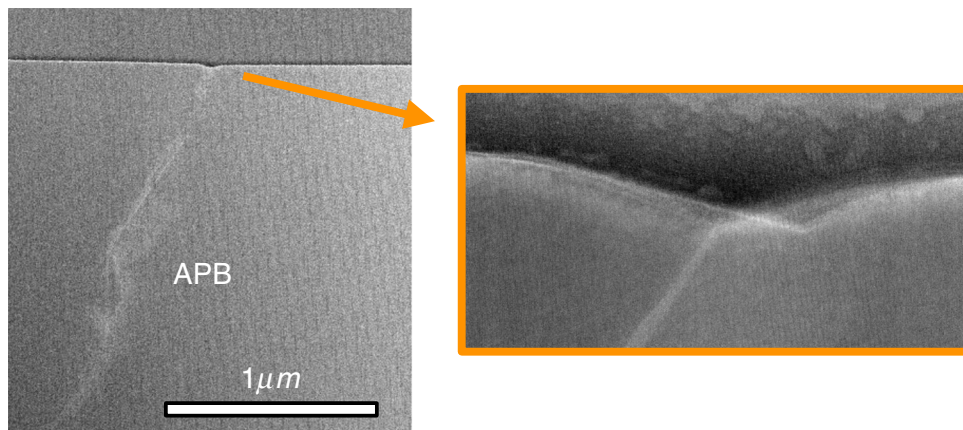


FIG. 3. (left) Scanning transmission electron microscopy image of an APB within a 3C-SiC (001) substrate. (right) Zoom of the surface depletion induced by the APB and lying at the (001) surface. It is worth noting that during the experimental growth along the [001] direction, the APB moves along the $\{110\}$ direction, reaching a final tilted configuration with respect to the (001) surface. The KMC evolution reported in Fig. 2 agrees quite well with the experimental analysis of this figure.

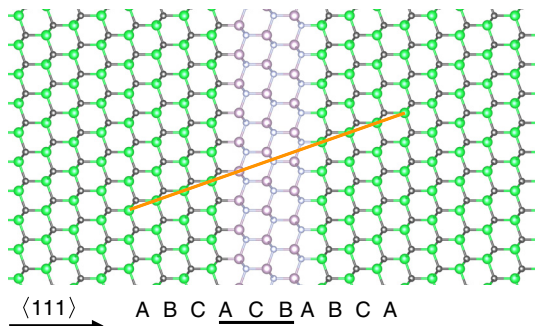


FIG. 4. Orthogonal view of a triple stacking fault SF(3): the faulted stacking sequence of the Si-C dimers along $\langle 111 \rangle$ directions with respect to the ideal ABC ABC ABC ... one is indicated with the light purple (silicon) and light blue (carbon) atoms; the orange line is a guide for the eye, highlighting the maintained epitaxial order in the two semi-spaces separated by the defect.

geometrical configuration of the supercell structures allowed for a direct contact between the metallic electrodes and the defects (see Fig. S2 of the [supplementary material](#)).

IV. RESULTS

The ideal conditions reproducing a flat substrate are difficult to achieve experimentally, since the initial substrate itself usually presents

non-homogeneous regions and preexisting defects. AntiPhase Domains (APDs) and related APBs are rather common defects when growing 3C-SiC crystals,¹ and they can form as possible boundaries of 3D structures merging in Volmer-Weber or Stranski-Krastanov growth modes.⁷⁰ A growing [e.g., (001)] surface with a preexisting extended defect (as the APB) exposes a defective region (linear “cut”), which can cause a disturbance on the growth kinetics. This growth kinetics unravels the eventual genesis, evolution, and interaction of extended defects (of various nature) starting from a defective seed layer.

We have considered a suitable model for the study of the kinetics of APBs within our KMCsL approach. At an atomic level, we introduce the APB as a planar distribution of anti-sites along a {110} crystal plane. At a mesoscopic level, we include four APBs, which reproduce a space distribution of APDs (considering the periodic boundary conditions imposed in the simulation box). This symmetric choice minimizes the possible artifacts caused in other possible configurations by periodic conditions and opposite phase domains. Green (silicon) and gray (carbon) atoms in [Fig. 1\(a\)](#) outline the four APBs and the different polarities of the substrate: considering the periodic boundary conditions on the xy plane, the substrate looks like an outline of APDs, favoring defect interactions in a reasonable time and space scale. Anti-sites along a {110} crystal plane are highlighted in [Figs. 1\(b\)](#) and [1\(c\)](#). [Figure 1\(c\)](#) represents the orthogonal view of a zoom of the APB showed in [Fig. 1\(b\)](#). Dashed and continuous segments of [Fig. 1\(c\)](#) highlight, respectively, the {111} Si-face and the C-face with the different

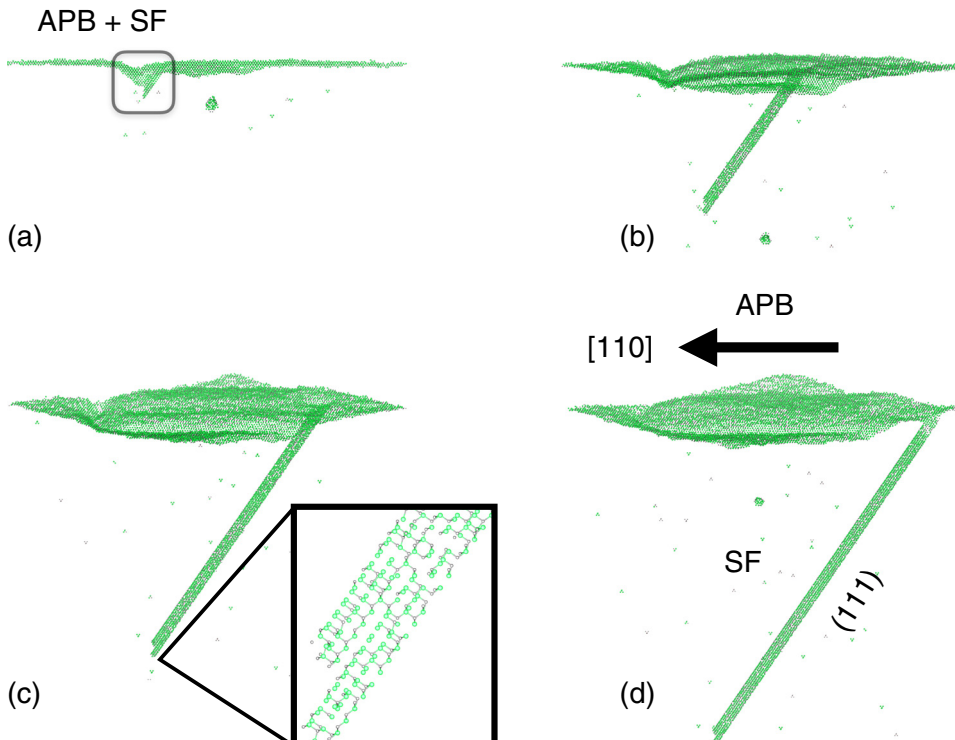


FIG. 5. Generation of a couple of triple stacking faults from the surface depletion induced by an APB during the 3C-SiC epitaxial growth along the [001] z direction. Under-coordinated atoms taken at different KMC times: (a) triple SFs generation from an APB (under-coordinated atoms related to the APB surface perturbation are visible); (b)-(d) three subsequent snapshots showing the independent kinetics of the APB moving toward the [110] direction, and the two generated triple SFs growing along (111) planes. The zoom in the (c) snapshot shows the three-bilayers structure of the two generated SF(3)s.

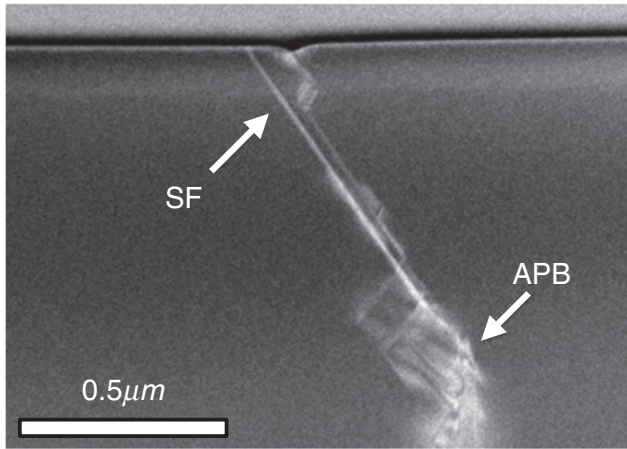


FIG. 6. Scanning transmission electron microscopy image of a stacking fault generated by an APB during the epitaxial growth of a 3C-SiC (001) substrate. It evolves on $\{111\}$ planes independently from the APB kinetics. The surface depletion is also visible at the terminal (001).

polarity. Note that no under-coordinated defects are present in the bulk of this structure, since the defective region is composed of planes with homoatomic Si–Si and C–C bonds.

The analysis reported in Secs. IV A–IV E discusses several representative features occurring randomly in the many-replicas of the KMCsL kinetics (in total we have investigated ~ 50 replicas of simulated evolution starting from the same initial state). We note that all figures in the paper refer to independent KMC runs where we modified only the input seed of the random number generator.

A. Antiphase boundary kinetics

Figure 2 reports the typical KMC evolution of a domain with four APBs along the $\{110\}$ planes during the 3C-SiC substrate growth

along the [001] z direction. Figure 2(a) shows only atoms at the APBs in the whole simulation box, where the initial 3C-SiC (001) substrate grows in the z direction. Initial symmetric APBs are visible at surface portions in Fig. 2(b). Contrarily to the ideal case, the presence of the APBs in the underlying bulk crystal significantly alters the morphology of the growing surface. Figures 2(b)–2(d) reveal under-coordinated atoms, highlighting the “running” (001) surface. We observe that the bulk antiphase boundaries generate surface local depletion, with the two facets oriented very close to two $\{111\}$ planes that originate from the $\langle 110 \rangle$ lines in the growing surface. For example, the APB on the (110) plane realizes a surface depletion with (111) and $(\bar{1}\bar{1}1)$ surfaces. Such depletion is formed at the start of the KMC deposition, as highlighted by Fig. 2(c).

The APBs show a clear drift with different direction of motion for the boundaries of different symmetry, as observed in Fig. 2(a). The depletion depth, as well as the drift velocity of the antiphase boundaries depend on the deposition conditions. The drift mechanism [represented by the red arrows of Figs. 1(c) and 2(d)] relies on the different velocity of the $\{111\}$ facets forming the groove. Indeed due to the phase change induced by the APB, these facets are of opposite polarity (i.e., C-face and Si-face). Dashed and continuous segments in Fig. 2(d) highlight, respectively, the $\{111\}$ Si-face and the C-face forming the surface depletion at the APB. $\{111\}$ Si-face and C-face are also emphasized in Fig. 1(c).

In our deposition condition, C-faces have different growth velocity with respect to Si-faces (see Sec. S1 of the [supplementary material](#)). As a consequence of this non-symmetric APB kinetics, the APB gradually switches from a square shape to an elongated one as shown by the final KMC snapshot of Fig. 2(d).

In Fig. 3, we show a scanning transmission electron microscopy image of an APB within a 3C-SiC (001) substrate. It is worth noting that during the experimental growth along the [001] direction, the APB moves along the $\langle 110 \rangle$ direction, reaching a final tilted configuration with respect to the (001) surface. Figure 3 also provides a zoom of the surface depletion induced by the APB and lying at the (001) surface. The KMC evolution reported in Fig. 2 agrees quite well with the experimental analysis of Fig. 3.

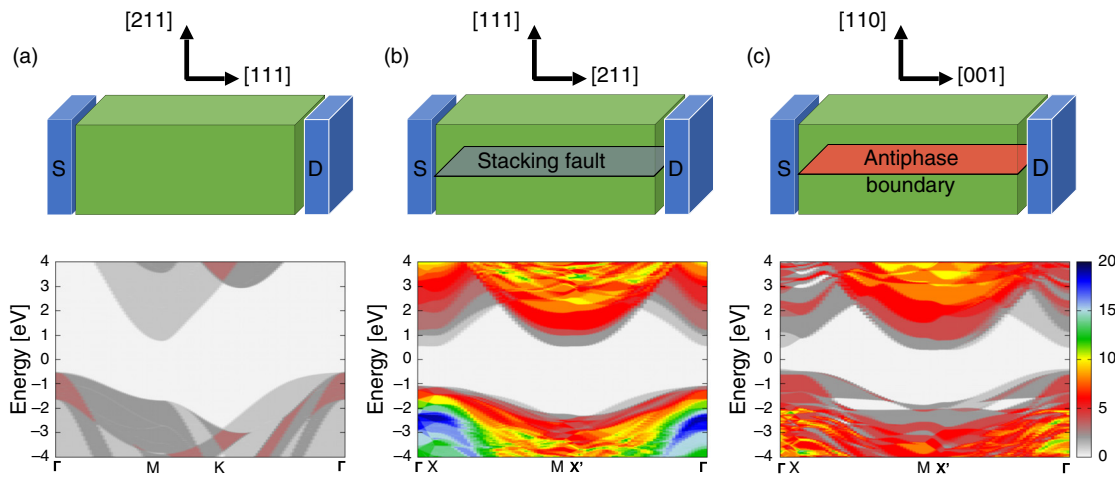


FIG. 7. Quantum transport in the reciprocal space for (a) nondefected 3C-SiC, (b) 3C-SiC with a triple stacking fault, and (c) 3C-SiC with an antiphase boundary. The color scale refers to the values of the transmission coefficient T that can be linked to the conductance through the Landauer formula, $G = G_0 T$, where $G_0 \approx 77.5\mu\text{S}$ is the conductance quantum.

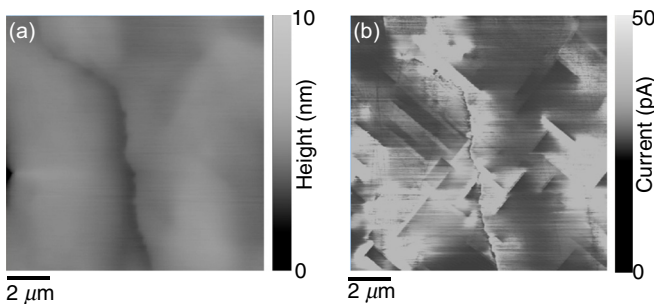


FIG. 8. (a) Conductive atomic force microscopy morphology and (b) current map collected on the surface of a 3C-SiC on Si sample by applying a positive bias ($V_{\text{tip}} = 0.5$ V) to the Pt tip. The presence of the APB is clearly visible as dark contrast in the morphology map in (a) due to the surface dip related to its presence; while both the APB and the associated SFs affect the local conductance as indicated by the bright contrast in the image (b).

B. Generation and kinetic stability of triple Stacking Faults

SFs are common and abundant extended defects in silicon carbide due to the similar energetics of different polytypes in such material. They can be easily categorized as wrong sequences with respect to the stacking order of the polytype in consideration.^{1,71} In the purely hexagonal close packed (hcp) representation, the polytype order is the periodic sequence of layers, composed of Si-C dimers along the hexagonal axis, where dimers in a single layer occupy one of the three highly symmetric positions usually named A, B, or C. The cubic 3C-SiC (zinc-blend) structure is obtained when the periodic sequence is ABC ABC ABC ..., which lies on the crystal {111} directions. As a consequence, the presence of {111} planes on the surface depletion allow for the generation of SFs.^{5,52}

A triple stacking fault SF(3) is characterized by three bi-layers that are not in the ideal crystal configuration. Figure 4 represents an orthogonal view of an SF(3): we note that the stacking sequence of a

triple SF (also known by the term “micro-twin,” ABC ACB ABC) separates two crystal regions in a perfectly epitaxial order, whereas the only atoms that are not in the correct crystal positions are those inside the extended defect.⁵² The faulted stacking sequence of the Si-C dimers along {111} directions with respect to the ideal periodic sequence, ABC ABC ABC ..., is indicated by the light purple (silicon) and light blue (carbon) atoms. The orange line is a guide for the eye, highlighting the maintained epitaxial order in the two semi-spaces separated by the defect.

Figure 5(a) shows the generation of a couple of triple stacking faults from the surface depletion induced by an APB. Figures 5(b)–5(d) represent a sequence of snapshots for the under-coordinated atoms taken at different KMC times. The triple SFs are visible in this representation due to the presence of tree-fold coordinated Monte Carlo particles at their boundary (i.e., at the associated partial dislocation). The zoom in Fig. 5(c) shows the three-bilayers structure of the two generated SF(3)s.

The local asymmetry of the APB and the presence of {111} facets on the surface depletion causes (due to polytype instability) the generation of triple SFs [see Figs. 5(a) and 5(b)]. Once the SF(3)s are generated by the APB, the two extended defect-types (SF(3)s and APB) follow independent kinetics: the APB continues its drift along the [110] direction, while the SF(3)s grow on the {111} planes [see snapshots of Figs. 5(b)–5(d)]. SF(3)s hold an elongated shape as shown in Fig. 9(e).

Figure 6 shows a scanning transmission electron microscopy image of a stacking fault generated by an APB during the epitaxial growth of a 3C-SiC (001) substrate. It evolves on {111} planes independently from the APB kinetics. The surface depletion is also visible at the terminal (001).

Figure 7 shows the calculated quantum transport properties of a triple stacking fault and an antiphase boundary, and compares them with the values expected for non-defected 3C-SiC. Both defects show an increased conductivity with respect to the ideal crystal due to an enhanced density of states at the defect area (see Fig. S3 of the supplementary material). Additionally, the antiphase boundary introduces

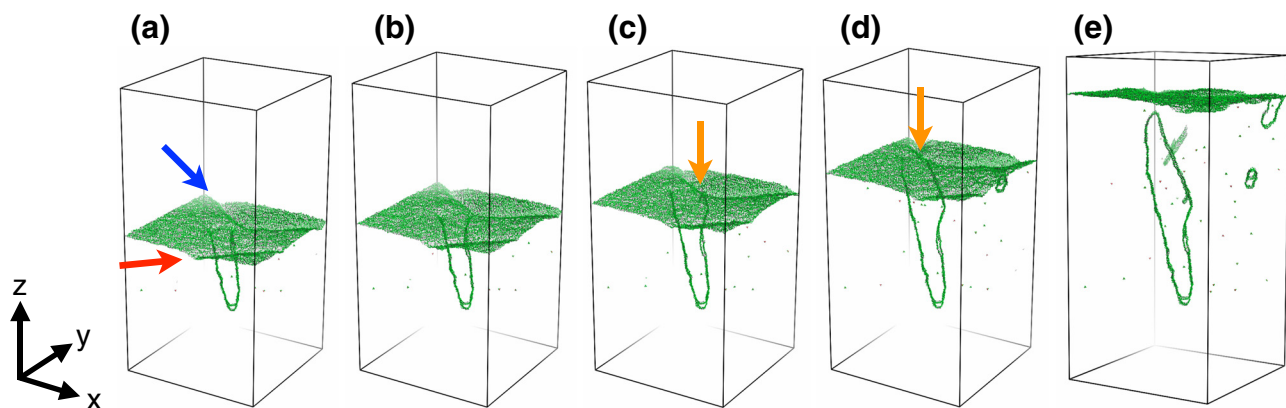


FIG. 9. Generation and termination of a couple of triple stacking faults from an antiphase boundary during the 3C-SiC epitaxial growth along the [001] z direction. Under-coordinated atoms taken at different KMC times: (a) SF(3)s growth along {111} planes during the epitaxial process: the red arrow highlights the APB that generated the SF(3)s, while the blue arrow points to the coming APB, which suppresses the SF(3)s; (b) contact between the SF(3)s and the APB moving along {110} directions; (c)-(d) two subsequent snapshots showing the growth termination of the SF(3)s induced by the APB evolution: orange arrows highlight the contact points between the APB and the SF(3)s; and (e) final snapshot with the SF(3)s closure. Multimedia view: <https://doi.org/10.1063/1.5132300.1>

states within the 3C-SiC bandgap that narrow the conduction gap. The large transmission coefficients of these defects as compared to the bulk indicates that both should be extremely conductive when contacted by the metallic electrodes. On the contrary, their effect on the transport properties should be restrictive when not in direct contact with the electrodes and perpendicular to the transport direction.⁶⁶ In that case, they should act as potential barriers hindering the conduction of current.

Figures 8(a) and 8(b) show a representative morphological image and the corresponding current map collected on the 3C-SiC surface by applying a DC bias of 0.5 V to the tip. The boundary between two neighboring domains can be observed in the morphological map [see Fig. 8(a)]. On the other hand, a large density of conductive features, mostly uncorrelated to the topography, is revealed by the current map in Fig. 8(b) and reflects the conductivity of APBs and SFs. The structural properties of these extended defects connecting the surface to the bulk of 3C-SiC layers will be extensively discussed in this paper. This preliminary electrical investigation clearly indicates how the presence of such a high density of conductive paths can have strong implications on the performances of vertical or quasi-vertical devices based on heteroepitaxial 3C-SiC on Si.⁵⁸ As an example, they can account for the typically low values of the turn-on voltage and the high leakage current observed in metal/3C-SiC Schottky barrier diodes.⁵⁶

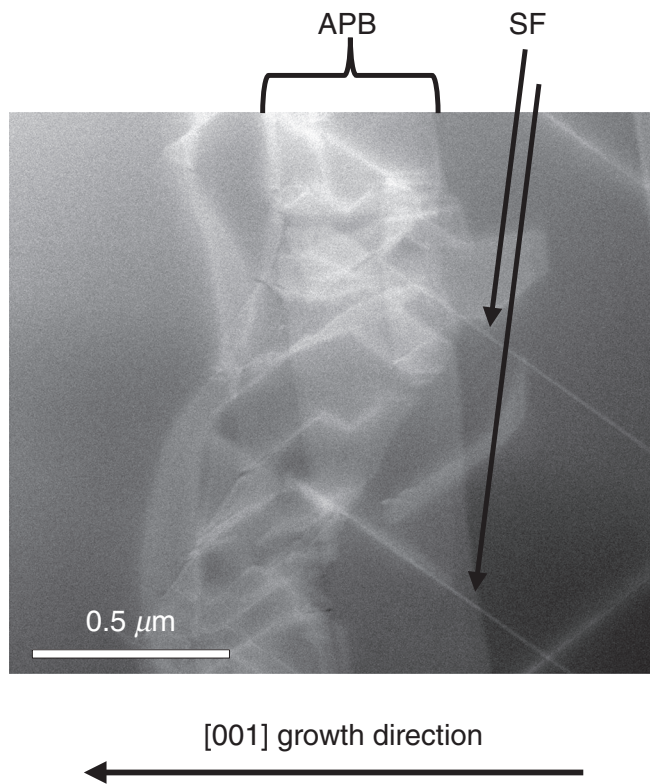


FIG. 10. Scanning transmission electron microscopy image showing the growth termination of triple stacking faults at a defective antiphase boundary during the epitaxial growth of a 3C-SiC (001) substrate.

C. SF(3)-APB interference: Growth termination and polarity changes of triple SFs

After its generation, an SF(3) can continue its extension during the epitaxial process at the 3C-SiC (001) surface, eventually increasing its size longitudinally (i.e., moving the partial dislocations that bind the SF(3) on the slipping plane). In the case of the triple SF, which perturbs minimally the crystal order of the embedding crystal, the defect's evolution is essentially driven by atomistic transitions occurring at the growing surface. The analysis of several equivalent replicas of the simulated kinetics seems to indicate that the persistence and enlargement of the SF(3) is ruled by a critical nucleation phenomenon: thanks to random fluctuations only defects that reach a critical lateral size manage to survive and extend during the simulated growth. However, the high kinetic (meta)stability of large SF(3)s is significantly hampered if

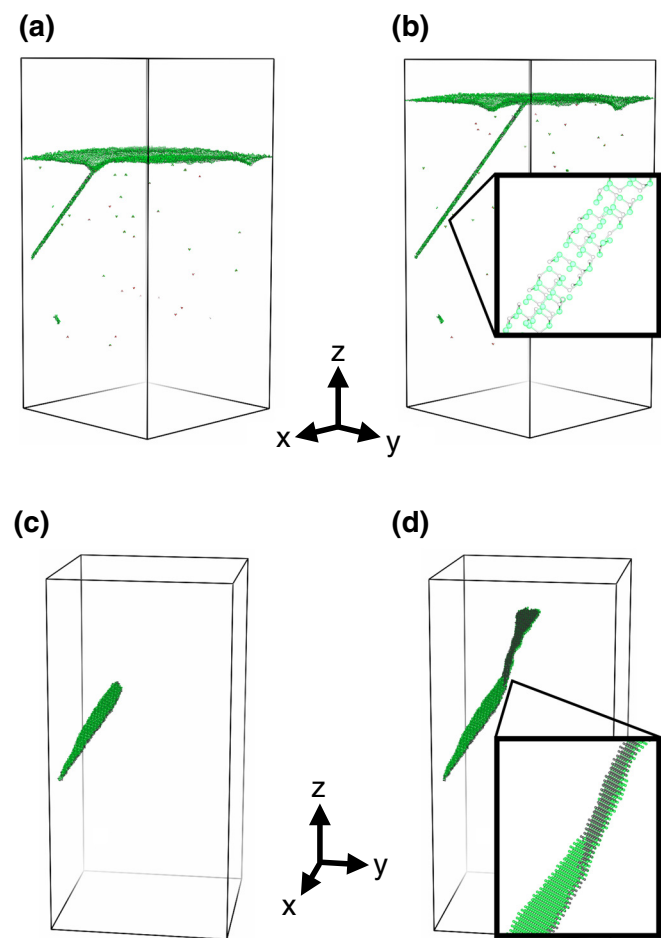


FIG. 11. Polarity change of a triple SF following its interaction with a moving APB during the 3C-SiC epitaxial growth along the [001] z direction. Under-coordinated atoms taken at different KMC times: (a) interaction between the SF(3) and an APB; (b) independent kinetics of the APB moving toward the $[1\bar{1}0]$ direction, and the triple SF turning away from the APB along (111) planes; (c) and (d) show atoms that are not epitaxially ordered and associated with the triple SF of (a) and (b), respectively. A zoom of the triple SF and the region where the polarity change takes place are also shown in the (b) and (d) snapshots, respectively.

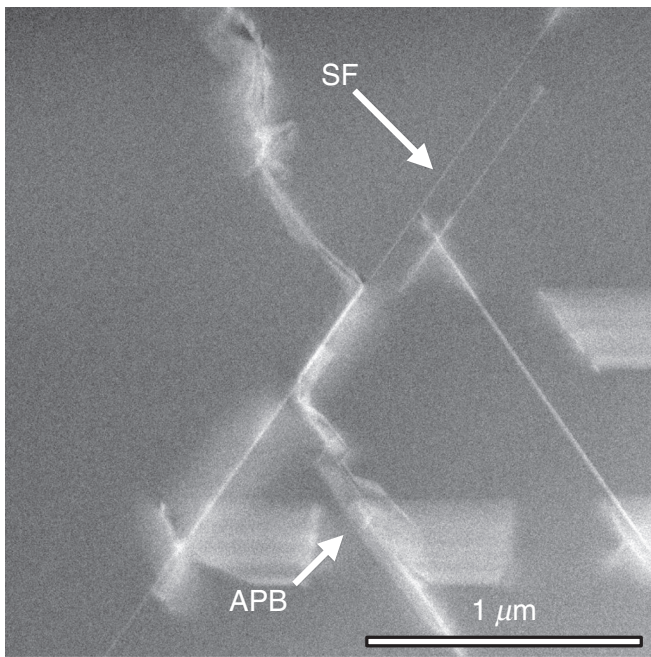


FIG. 12. Scanning transmission electron microscopy image showing the interaction between a stacking fault and a grain boundary during the epitaxial growth of a 3C-SiC (001) substrate.

another extended crystal imperfection interferes with the defect evolution.

In particular, we investigated this defect-defect interaction, thanks to the presence of multiple APBs in the same KMC framework. As a possible result of this extended defects interaction, we observed both SF $\langle 3 \rangle$ growth termination and survival (followed by a polarity change) due to a different APB coming from the orthogonal direction to the original APB that generated the SF $\langle 3 \rangle$.

Figure 9 illustrates the whole process of the SF $\langle 3 \rangle$ growth suppression (Multimedia view). A couple of triple SFs are generated at the surface depletion induced by an antiphase boundary [Fig. 9(a)]. Then they come in contact with another APB orthogonal to the APB that generated the two SF $\langle 3 \rangle$ s [Fig. 9(b)]. The red arrow of Fig. 9(a) highlights the APB that generated the SF $\langle 3 \rangle$ s, while the blue arrow points to the coming APB, which suppresses the SF $\langle 3 \rangle$ s. The SF $\langle 3 \rangle$ s growth is then suppressed (in this case) by the APB, as shown by snapshots in Figs. 9(c) and 9(d), taken at subsequent times (orange arrows highlight the contact points between the APB and the SF $\langle 3 \rangle$ s). Finally, driven by the APB drift along the [1̄10] direction, the SF $\langle 3 \rangle$ s close, and the crystal surface is healed [see Fig. 9(e)]. A movie of the KMC evolution described in Fig. 9 is reported in the supplementary material. Figure 9(e) also shows small SF $\langle 3 \rangle$ s that are generated and immediately closed. It is worth recalling now that SF $\langle 3 \rangle$ s and the associated partial dislocations cannot be self-terminated, whereas either the generation or the termination of SF $\langle 3 \rangle$ s is always connected with the presence of a domain boundary. The generation and termination processes are stochastic in nature, due to the isoenergetic configurations of 3C-SiC, and depend on the local epitaxial growth at an atomistic level.

KMC results for the growth termination of triple SFs at defective domain boundaries agree with experimental observations of the epitaxial growth of 3C-SiC antiphase domains. Figure 10 provides a scanning transmission electron microscopy image showing the growth termination of various SF $\langle 3 \rangle$ s at a defective antiphase boundary during the epitaxial growth of a 3C-SiC (001) substrate. Both SF $\langle 3 \rangle$ s and APB defects show independent kinetics during the epitaxial growth. Once they come in contact, the SF $\langle 3 \rangle$ s disappear. *A posteriori* experimental characterization is not able to reveal the mechanism beyond their interaction, which, conversely, can be easily deduced from the KMC simulation.

Another kind of behavior can be observed from the KMC simulations: an SF $\langle 3 \rangle$ can continue its extension during epitaxial growth, surviving from the interaction with an APD boundary by changing its polarity. Figure 11 illustrates the polarity change of a triple SF

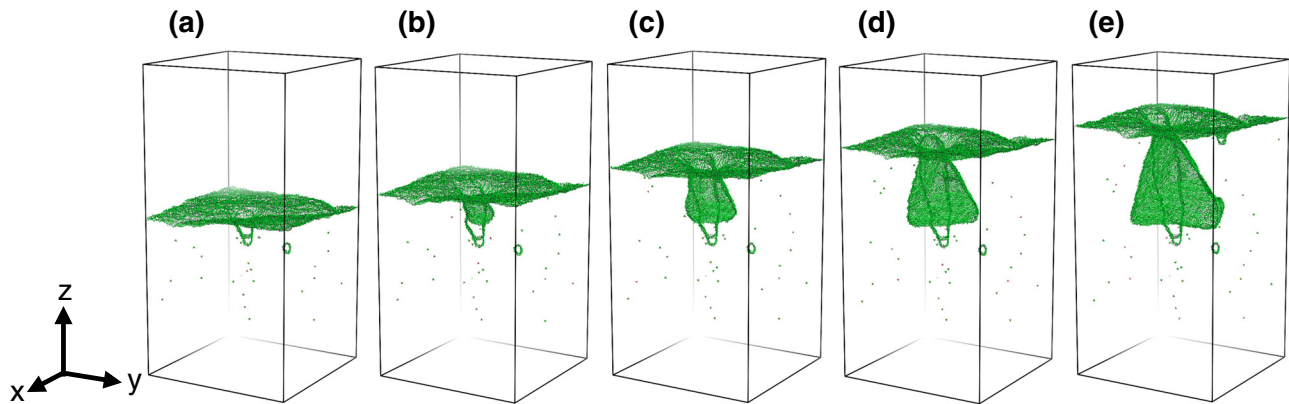


FIG. 13. Generation and bulk growth of a single stacking fault from an antiphase boundary during the 3C-SiC epitaxial growth along the [001] z direction. Under-coordinated atoms taken at different KMC times: (a) formation of two triple SFs from the APB during the epitaxial process; (b) formation of a single SF from the APB aligned to the previous triple SFs; (c)-(e) three subsequent snapshots showing the growth of the SF tetrahedra starting from the single SF in the bulk 3C-SiC crystal, while the triple SFs mainly evolve only at the surface of the growing crystal.

following its interaction with a moving APB during the 3C-SiC epitaxial growth along the [001] z direction. We show under-coordinated atoms taken at different KMC times. First, the SF<3> interacts with the APB [see Fig. 11(a)]. The SF<3> survives and follows independent kinetics with respect to the APB [Fig. 11(b)]. The latter moves toward the [110] direction, while the triple SF instead turns away from the APB along the (111) planes. To highlight the SF polarity change, we show in Figs. 11(c) and 11(d) the atoms that are not epitaxially ordered and associated, respectively, to the triple SF of Figs. 11(a) and 11(b). The zoom in Figs. 11(b) and 11(d) highlights the triple stacking fault and the region where the polarity change takes place, respectively.

The original plane of the SF<3> does not change since a polarity change involves only a local reversal of the Si-C doublet. So the original plane of the SF, in the reference system of the initial substrate, remains the (111) plane. For similar reasons, the stacking sequence does not change once the SF passes from a crystal domain to another crossing an APB. The basal plane dislocations at the boundary of the stacking faults, which disappear by crossing in the case of SFs' growth termination [see Figs. 9(c)–9(e)], react in the case of polarity change and modify their atomic configuration. This modification of the bonding network can be described by a direction change of the dislocation vectors within the SF<3> habit plane and an inversion Si-C \Rightarrow C-Si of the defects' pairs (due to the polarity change) along the dislocations' direction.

Figure 12 shows a scanning transmission electron microscopy image that reveals the interaction between a triple stacking fault with a grain boundary. It is apparent that an SF<3> belonging to the crystal on the left side encounters the APB and emerges in the crystal on the right side. Although it is impossible to detect the polarity change of the SF, we note its survival after the interaction with an APB, and its subsequent independent kinetics with respect to the APB.

D. Generation and bulk growth of SF(1) tetrahedra

The similar energetics of different SiC polytypes can accommodate a large family of extended defects, characterized by various wrong stacking sequences with respect to the cubic polymorph. As a result, very complex behavior can also be obtained. Three dimensional arrangements of SFs called SF tetrahedra (SF(T)) can be generated. They are constituted by 4 intrinsic single SFs (SF(1), i.e., SF with a single wrong sequence⁵²) limited by stair rod dislocations forming a tetrahedron.⁷² An SF(T) can originate on the {111}-oriented surface depletion induced by an APB, in a similar way to SF<3>'s reported in Secs. IV B and IV C. Figure 13 shows the generation of a single stacking fault from an APB and the bulk growth of the SF tetrahedron. Initially, the epitaxial growth produces two consecutive triple SFs at the APB [Fig. 13(a)]. Then, the same APB in Fig. 13(b) generates a single SF [aligned to the previous triple SFs, i.e., lying on the (111) plane]. Differently from the triple SF, the single SF has a non-negligible Burgers vector and separates the crystal into two regions that are not in perfect epitaxial arrangement. As a consequence, an SF with finite size, transmits this atomic misalignment along its border, which in turn becomes a mobile interface in the crystal that rearranges itself. Hence, the SF(T) expands, while the apical part of the defect grows, following the surface motion.

The atomistic KMCsL code is able to reproduce the bulk expansion of this portion related to finite size single SFs. Snapshots of

Figs. 13(c)–13(e) show the growth of the SF tetrahedron in the bulk 3C-SiC crystal, while the triple SF mainly evolves only at the surface of the growing crystal. In the same KMC framework, we can unravel the opposite behaviors of the extended defects and triple SFs. The first can expand in the bulk with independent kinetics from the superficial epitaxial growth, while the second, once generated at the {111} planes

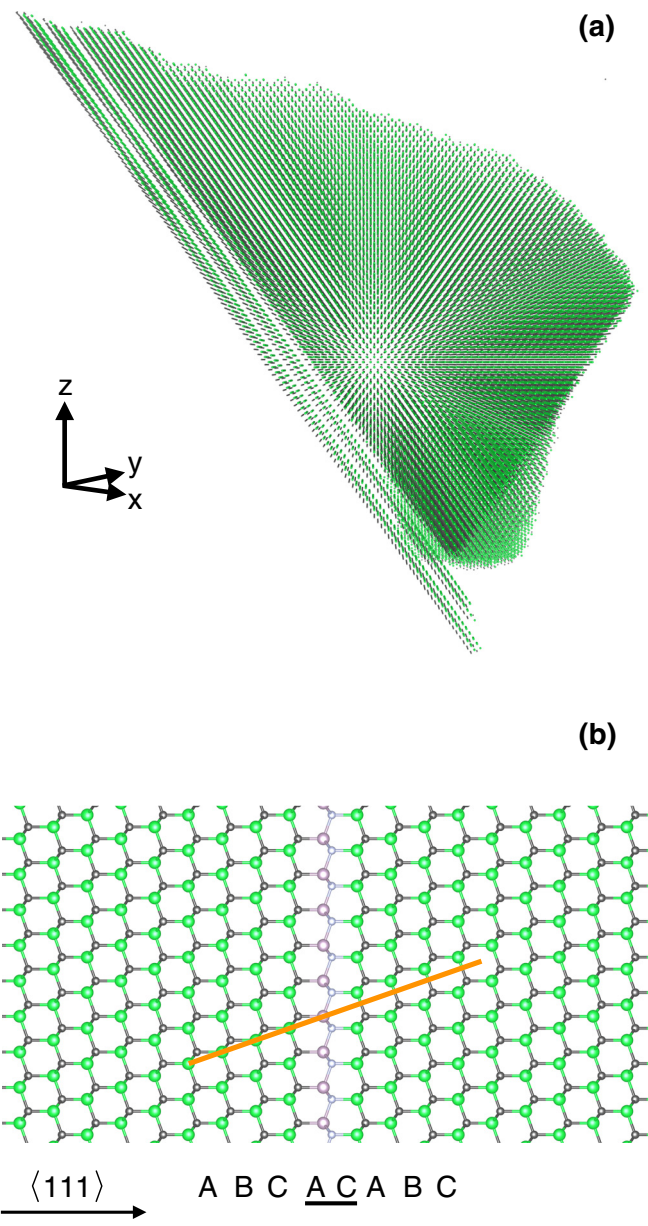


FIG. 14. (a) Lateral view along the [110] direction of the extended defect shown in Fig. 13(e); atoms that are not epitaxially ordered, representing the single and triple SFs; (b) orthogonal view of a single stacking fault SF(1): the faulted stacking sequence of the Si-C dimers along (111) directions with respect to the ideal ABC ABC ABC ... one is indicated; the orange line is a guide for the eye, highlighting the non-maintained epitaxial order in the two semi-spaces separated by the defect.

of the APB depletion, maintains a fixed shape. It is interesting to note that the SF $\langle T \rangle$ adapts the edges on [110] directions. It is known that the edges of the SF $\langle T \rangle$ are stair-rod dislocations,⁷² which suggests that partial dislocations tend to be straight and with screw character.

Figure 14(a) shows a lateral view along the [110] direction of the snapshot of Fig. 13(e). It indicates atoms that are not epitaxially ordered, representing the single and triple SFs. Figure 14(b) represents a cartoon with the orthogonal view of a single stacking fault SF $\langle 1 \rangle$ with a stacking sequence of ABC AC ABC. The faulted stacking sequence of the Si–C dimers along {111} directions with respect to the ideal ABC ABC ABC ... one is indicated. An SF $\langle 1 \rangle$ does not maintain any epitaxial order in the two semi-spaces separated by the defect as highlighted by the orange line crossing the extended defect. Please note that a possible microscopy analysis in cross section mode of this defective volume will appear as a triple SF sequence and two split SF $\langle 1 \rangle$ s, which form two edges of the SF $\langle T \rangle$. Therefore, the KMCsL simulation can unravel the kinetic mechanism underlying some experimental evidence obtained by means of transmission electron microscopy.

E. Multiple sequence of triple SFs

As shown in Figs. 5, 9, and 13, triple stacking faults can be generated by the APB in sequence (two consecutive triple SFs are present in these cases). Figure 15 demonstrates the generation of a multiple sequence of triple SFs from an APB during 3C-SiC epitaxial growth along the [001] z direction. Under-coordinated atoms taken at different KMC times have been selected. In particular, Fig. 15(a) shows the formation of the first triple SF. The APB continues to generate adjacent triple SFs as illustrated in the snapshots of Figs. 15(b)–15(e). This continuous sequence of triple SFs represents a local nanocrystal domain with sequence ABC ABC ACB ACB ... (that is an extended twin configuration). A further consequence of such a triple SF sequence is a local rectangular depletion at the growing (001) surface.

Figure 16(a) shows a lateral view along the [110] direction of the snapshot of Fig. 15(e). We select atoms that are not epitaxially ordered

representing the multiple sequence of triple SFs. We also show in Fig. 16(b) a cartoon representing the orthogonal view of a multiple sequence of triple stacking faults SF $\langle 3 \rangle$ s. The faulted stacking sequence of the Si–C dimers along {111} directions with respect to the ideal ABC ABC ABC ... one is indicated. The orange line is a guide for the eye, highlighting the epitaxial order in the two semi-spaces where just one of three bilayers of ABC represented by the dark purple (silicon) and dark blue (carbon) atoms follows the stacking sequence of the 3C-SiC crystal.

V. CONCLUSIONS

This work has been motivated by the quest for a deeper control of material quality in one of the most promising semiconductors for future power electronic devices, i.e., the cubic polymorph of SiC. Indeed, the high number of defects characterizing the material obstructs its high potential in, e.g., 3C-SiC power MOSFETs, where the 3C-SiC superior physical properties could increase the performance with respect to current state-of-the-art power devices.

In spite of recent intense research focusing on the improvement of the 3C-SiC material, only incremental results have been achieved so far. We have indicated that these difficulties could also derive from the lack of complete understanding of the mechanisms ruling the generation, evolution, and interaction of extended defects in SiC. Indeed, the kinetics of defective SiC systems has been subjected to partial and often qualitative theoretical analyses, whereas experimental investigations provide an accurate description of the material status only after the synthesis process. Likely, they do not have access to the microstructural evolution during the process itself.

The results discussed demonstrate that the combination of advanced simulation methodologies and experimental characterization techniques closes this knowledge gap. We would like to summarize the main scientific achievements of the research presented here. First, in terms of theoretical and computational research, we have demonstrated that long-time kinetics of complex systems (all the examples discussed refer to growths lasting several minutes) can be predicted and

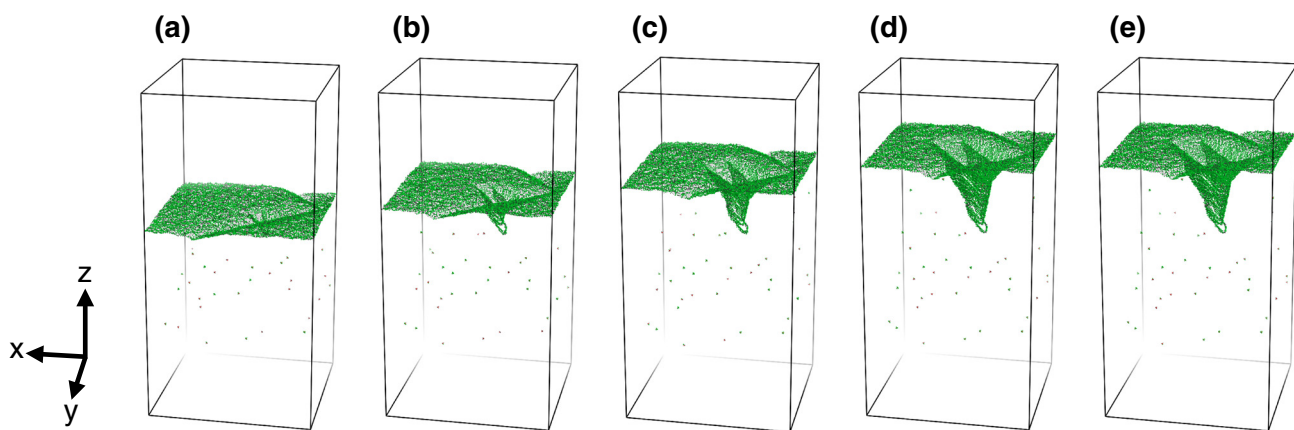


FIG. 15. Generation of a multiple sequence of triple SFs from an antiphase boundary during the 3C-SiC epitaxial growth along the [001] z direction. Under-coordinated atoms taken at different KMC times: (a) formation of the first triple SF; (b)–(e) four subsequent snapshots showing the generation of multiple triple SFs, and the consequent surface depletion.

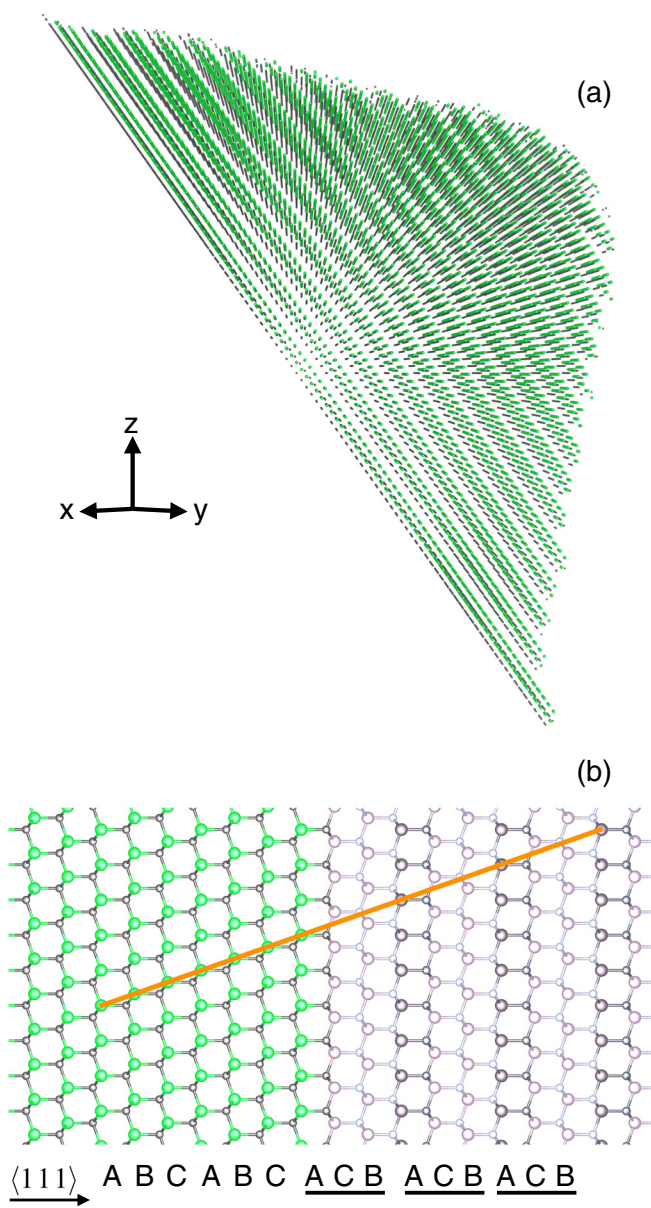


FIG. 16. (a) Lateral view along the $\langle\bar{1}10\rangle$ direction of the extended defect shown in Fig. 15(e); atoms that are not epitaxially ordered, representing the multiple sequence of triple SFs; (b) orthogonal view of a multiple sequence of triple stacking faults SF $\langle 3 \rangle$ s: the faulted stacking sequence of the Si-C dimers along $\langle 111 \rangle$ directions with respect to the ideal ABC ABC ABC ... one is indicated; the orange line is a guide for the eye, highlighting the epitaxial order in the two semi-spaces where just one of the three ABC bilayers, indicated by the dark purple (silicon) and dark blue (carbon) atoms, follows the stacking sequence of the 3C-SiC crystal.

analyzed with atomic resolution. The accuracy of the method relies on an *ab initio* calibration and can be directly evaluated by the experiments, since it virtually reproduces equivalent growth conditions.

As a relevant general outcome for materials science research, our investigations suggest that the processing of a defective system

does not provide univocal upshots. Indeed, a non-pre-definite branching of the evolutive features in the 3C-SiC growths has been theoretically and experimentally evidenced. In particular, the stochastic simulation analysis, which was initiated exactly with the same defective APD system and with the same growing conditions, demonstrates without any doubts that this branching is “intrinsic” and not dependent on the possible experimental variance of the initial state.

For specialists in the growth processes of SiC materials, our results identify a critical source of other extended defects in the anti-phase boundary; therefore, the control of APBs and their eventual reduction is particularly important for achieving a good quality of the grown crystals. We have shown, by means of combined conductivity measurements with nanoscale resolution and quantum transport calculations, that the association of APBs and SFs strongly alters the surface conductive paths and can have a detrimental impact on the performances of vertical or quasi-vertical devices based on heteroepitaxial 3C-SiC on Si.

Finally, since the atomic mechanisms at the basis of extended defect evolution are accessible by the method, several particular aspects have been analyzed and discussed in Sec. IV. We have shown how the interaction of different types of defects often derives from the rearrangement of the atomic configuration of the defect portion emerging at the growing surface, whose morphology is in turn affected by the defect proximity. We would like to advise the reader that surface mediated interactions are an important, but partial aspect of the defect-defect correlation modes. Indeed, defect induced instabilities could give rise to “pure bulk” kinetics, which can be accessed by the *ab initio* calibrated KMCsL approach and will be investigated in the future.

SUPPLEMENTARY MATERIAL

See the [supplementary material](#) for the following: calibration details of the KMCsL code (Sec. S1) and KMC results for the epitaxial growth of an ideal 3C-SiC (001) substrate (Sec. S2); and details for the quantum transport calculations (Sec. S3). The movie SF-APB-generation-growth-termination.mp4 shows the generation and termination of a couple of triple stacking faults from an APB during the 3C-SiC epitaxial growth along the $[001]$ z direction.

ACKNOWLEDGMENTS

This work has been supported by the CHALLENGE project (HORIZON 2020-NMBP-720827, <http://www.h2020challenge.eu/>). CHALLENGE is a research and innovation action funded by the European Union’s Horizon 2020 program. Computer resources were provided by the Swiss National Supercomputing Center (CSCS) under Project ID s869.

REFERENCES

- ¹T. Kimoto and J. Cooper, *Fundamentals of Silicon Carbide Technology: Growth, Characterization, Devices and Applications* (John Wiley & Sons Singapore Pte. Ltd., 2014) pp. 1–538.
- ²J. Millán, P. Godignon, X. Perpiñà, A. Pérez-Tomás, and J. Rebollo, “A survey of wide bandgap power semiconductor devices,” *IEEE Trans. Power Electron.* **29**, 2155–2163 (2014).
- ³A. Lidow, M. de Rooij, J. Strydom, D. Reusch, and J. Glaser, *GaN Transistors for Efficient Power Conversion*, 3rd ed. (John Wiley & Sons, Ltd., 2019) pp. 1–384.

- ⁴F. Roccaforte, P. Fiorenza, G. Greco, R. L. Nigro, F. Giannazzo, A. Patti, and M. Saggio, "Challenges for energy efficient wide band gap semiconductor power devices," *Phys. Status Solidi A* **211**, 2063–2071 (2014).
- ⁵F. L. Via, M. Camarda, and A. La Magna, "Mechanisms of growth and defect properties of epitaxial SiC," *Appl. Phys. Rev.* **1**, 031301 (2014).
- ⁶D. G. Senesky, B. Jamshidi, K. B. Cheng, and A. P. Pisano, "Harsh environment silicon carbide sensors for health and performance monitoring of aerospace systems: A review," *IEEE Sens. J.* **9**, 1472–1478 (2009).
- ⁷P. Tanner, A. Iacopi, H.-P. Phan, S. Dimitrijević, L. Hold, K. Chaik, G. Walker, D. V. Dao, and N.-T. Nguyen, "Excellent rectifying properties of the n-3C-SiC/p-Si heterojunction subjected to high temperature annealing for electronics, MEMS, and LED applications," *Sci. Rep.* **7**, 17734 (2017).
- ⁸S. Nishino, J. A. Powell, and H. A. Will, "Production of large-area single-crystal wafers of cubic SiC for semiconductor devices," *Appl. Phys. Lett.* **42**, 460–462 (1983).
- ⁹M. Reyes, Y. Shishkin, S. Harvey, and S. E. Saddow, "Development of a high-growth rate 3C-SiC on Si CVD process," *MRS Proc.* **911**, 0911-B08-01 (2006).
- ¹⁰M. Zielinski, S. Ndiaye, T. Chassagne, S. Juillaguet, R. Lewandowska, M. Portail, A. Leycuras, and J. Camassel, "Strain and wafer curvature of 3C-SiC films on silicon: Influence of the growth conditions," *Phys. Status Solidi A* **204**, 981–986 (2007).
- ¹¹A. Severino, C. Bongiorno, N. Piluso, M. Italia, M. Camarda, M. Mauceri, G. Condorelli, M. D. Stefano, B. Cafra, A. L. Magna, and F. L. Via, "High-quality 6-inch (111) 3C-SiC films grown on off-axis (111) Si substrates," *Thin Solid Films* **518**, S165–S169 (2010).
- ¹²J. Yamasaki, S. Inamoto, Y. Nomura, H. Tamaki, and N. Tanaka, "Atomic structure analysis of stacking faults and misfit dislocations at 3C-SiC/Si(001) interfaces by aberration-corrected transmission electron microscopy," *J. Phys. D: Appl. Phys.* **45**, 494002 (2012).
- ¹³G. Litrico, R. Anzalone, A. Alberti, C. Bongiorno, G. Nicotra, M. Zimbone, M. Mauceri, S. Coffa, and F. La Via, "Stacking faults defects on 3C-SiC homo-epitaxial films," in *Silicon Carbide and Related Materials 2017*, Materials Science Forum, Vol. 924 (Trans Tech Publications Ltd, 2018) pp. 124–127.
- ¹⁴W. T. Read and W. Shockley, "Dislocation models of crystal grain boundaries," *Phys. Rev.* **78**, 275–289 (1950).
- ¹⁵L. Pelaz, M. Jaraiz, G. H. Gilmer, H.-J. Gossmann, C. S. Rafferty, D. J. Eaglesham, and J. M. Poate, "B diffusion and clustering in ion implanted Si: The role of B cluster precursors," *Appl. Phys. Lett.* **70**, 2285–2287 (1997).
- ¹⁶P. Pichler, *Intrinsic Point Defects, Impurities, and Their Diffusion in Silicon* (Springer-Verlag Wien, 2004) pp. 1–554.
- ¹⁷J. Thibault, J.-L. Rouvire, and A. Bourret, "Grain boundaries in semiconductors," in *Materials Science and Technology* (American Cancer Society, 2013).
- ¹⁸V. V. Voronkov and R. Falster, "Intrinsic point defects and impurities in silicon crystal growth," *J. Electrochem. Soc.* **149**, G167–G174 (2002).
- ¹⁹T. Kimoto, "Bulk and epitaxial growth of silicon carbide," *Prog. Cryst. Growth Charact. Mater.* **62**, 329–351 (2016).
- ²⁰F. L. Via, A. Severino, R. Anzalone, C. Bongiorno, G. Litrico, M. Mauceri, M. Schoeler, P. Schuh, and P. Wellmann, "From thin film to bulk 3C-SiC growth: Understanding the mechanism of defects reduction," *Mat. Sci. Semicon. Proc.* **78**, 57–68 (2018).
- ²¹H. Matsunami, "Growth and application of cubic SiC," *Diam. Relat. Mater.* **2**, 1043–1050 (1993).
- ²²W. Wesch, "Silicon carbide: Synthesis and processing," *Nucl. Instrum. Methods Phys. Res. B* **116**, 305–321 (1996).
- ²³A. Fissel, "Artificially layered heteropolytypic structures based on SiC polytypes: Molecular beam epitaxy, characterization and properties," *Phys. Rep.* **379**, 149–255 (2003).
- ²⁴W. J. Choyke, H. Matsunami, and G. Pensl, *Silicon Carbide - Recent Major Advances* (Springer, Berlin, Heidelberg, 2004) pp. 1–899.
- ²⁵T. Kimoto and H. Matsunami, "Surface kinetics of adatoms in vapor phase epitaxial growth of SiC on 6H-SiC{0001} vicinal surfaces," *J. Appl. Phys.* **75**, 850–859 (1994).
- ²⁶S. T. Dunham and C. D. Wu, "Atomistic models of vacancy-mediated diffusion in silicon," *J. Appl. Phys.* **78**, 2362–2366 (1995).
- ²⁷M. M. Bunea and S. T. Dunham, "Monte Carlo study of vacancy-mediated impurity diffusion in silicon," *Phys. Rev. B* **61**, R2397–R2400 (2000).
- ²⁸L. Pelaz, L. A. Marqués, and J. Barbolla, "Ion-beam-induced amorphization and recrystallization in silicon," *J. Appl. Phys.* **96**, 5947–5976 (2004).
- ²⁹M. Camarda, A. L. Magna, P. Fiorenza, F. Giannazzo, and F. L. Via, "Defect formation and evolution in the step-flow growth of silicon carbide: A Monte Carlo study," *J. Cryst. Growth* **310**, 971–975 (2008).
- ³⁰S. Roy, M. Portail, T. Chassagne, J. M. Chauveau, P. Vennéguès, and M. Zielinski, "Transmission electron microscopy investigation of microtwins and double positioning domains in (111) 3C-SiC in relation with the carbonization conditions," *Appl. Phys. Lett.* **95**, 081903 (2009).
- ³¹G. Fisicaro, L. Pelaz, P. Lopez, and A. La Magna, "Kinetic Monte Carlo simulations for transient thermal fields: Computational methodology and application to the submicrosecond laser processes in implanted silicon," *Phys. Rev. E* **86**, 036705 (2012).
- ³²G. Fisicaro, L. Pelaz, M. Aboy, P. Lopez, M. Italia, K. Huet, F. Cristiano, Z. Essa, Q. Yang, E. Bedel-Pereira, M. Quillec, and A. L. Magna, "Kinetic Monte Carlo simulations of boron activation in implanted Si under laser thermal annealing," *Appl. Phys. Express* **7**, 021301 (2014).
- ³³I. Deretzis and A. L. Magna, "Simulating structural transitions with kinetic Monte Carlo: The case of epitaxial graphene on SiC," *Phys. Rev. E* **93**, 033304 (2016).
- ³⁴M. Albani, L. Ghisalberti, R. Bergamaschini, M. Friedl, M. Salvaglio, A. Voigt, F. Montalenti, G. Tütüncüoglu, A. Fontcuberta i Morral, and L. Miglio, "Growth kinetics and morphological analysis of homoepitaxial GaAs fins by theory and experiment," *Phys. Rev. Mater.* **2**, 093404 (2018).
- ³⁵F. Gao, E. J. Bylaska, W. J. Weber, and L. R. Corrales, "Ab initio and empirical-potential studies of defect properties in 3C-SiC," *Phys. Rev. B* **64**, 245208 (2001).
- ³⁶D. C. Rapaport, *The Art of Molecular Dynamics Simulation*, 2nd ed. (Cambridge University Press, 2004).
- ³⁷A. Sarikov, A. Marzegalli, L. Barbin, F. Montalenti, and L. Miglio, "Structure and stability of partial dislocation complexes in 3C-SiC by molecular dynamics simulations," *Mater.* **12**, 3027 (2019).
- ³⁸S. Tan and P.-M. Lam, "Monte Carlo simulation of three-dimensional islands," *Phys. Rev. B* **60**, 8314–8320 (1999).
- ³⁹M. Biehl, F. Much, and, and C. Vey, "Off-lattice kinetic Monte Carlo simulations of strained heteroepitaxial growth," in *Multiscale Modeling in Epitaxial Growth*, edited by A. Voigt (Birkhäuser Basel, Basel, 2005) pp. 41–56.
- ⁴⁰P. J. Stout, "Modeling surface kinetics and morphology during 3C, 2H, 4H, and 6H-SiC (111) step-flow growth," *J. Vac. Sci. Technol. A* **16**, 3314–3327 (1998).
- ⁴¹N. Metropolis, A. W. Rosenbluth, M. N. Rosenbluth, A. H. Teller, and E. Teller, "Equation of state calculations by fast computing machines," *J. Chem. Phys.* **21**, 1087–1092 (1953).
- ⁴²M. Biehl, "Lattice gas models and kinetic Monte Carlo simulations of epitaxial growth," in *Multiscale Modeling in Epitaxial Growth*, edited by A. Voigt (Birkhäuser Basel, Basel, 2005) pp. 3–18.
- ⁴³C. C. Battaile, "The kinetic Monte Carlo method: Foundation, implementation, and application," *Comput. Meth. Appl. Mech. Eng.* **197**, 3386–3398 (2008).
- ⁴⁴M. Stamatakis, "Kinetic modelling of heterogeneous catalytic systems," *J. Phys. Condens. Matter* **27**, 013001 (2014).
- ⁴⁵M. Andersen, C. Panosetti, and K. Reuter, "A practical guide to surface kinetic Monte Carlo simulations," *Front. Chem.* **7**, 202 (2019).
- ⁴⁶J. D. Weeks, G. H. Gilmer, and K. A. Jackson, "Analytical theory of crystal growth," *J. Chem. Phys.* **65**, 712–720 (1976).
- ⁴⁷T. Volkmann, M. Ahr, and M. Biehl, "Kinetic model of II-VI(001) semiconductor surfaces: Growth rates in atomic layer epitaxy," *Phys. Rev. B* **69**, 165303 (2004).
- ⁴⁸M. Camarda, A. L. Magna, and F. L. Via, "A kinetic Monte Carlo method on super-lattices for the study of the defect formation in the growth of close packed structures," *J. Comput. Phys.* **227**, 1075–1093 (2007).
- ⁴⁹M. A. Załuska-Kotur and F. Krzyżewski, "Step bunching process induced by the flow of steps at the sublimated crystal surface," *J. Appl. Phys.* **111**, 114311 (2012).
- ⁵⁰H.-J. Guo, W. Huang, X. Liu, P. Gao, S.-Y. Zhuo, J. Xin, C.-F. Yan, X.-C. Liu, Y.-Q. Zheng, J.-H. Yang, and E.-W. Shi, "A competitive lattice model Monte Carlo method for simulation competitive growth of different polytypes in close-packed crystals: 4H and 6H silicon carbide," *Comput. Mater. Sci.* **100**, 159–165 (2015).

- ⁵¹T. Kimoto, "Material science and device physics in SiC technology for high-voltage power devices," *Jpn. J. Appl. Phys.* **54**, 040103 (2015).
- ⁵²A. La Magna, A. Alberti, E. Barbagiovanni, C. Bongiorno, M. Cascio, I. Deretzis, F. La Via, and E. Smecca, "Simulation of the growth kinetics in group IV compound semiconductors," *Phys. Status Solidi A* **216**, 1800597 (2019).
- ⁵³F. La Via, G. D'Arrigo, A. Severino, N. Piluso, M. Mauceri, C. Locke, and S. E. Saddow, "Patterned substrate with inverted silicon pyramids for 3C-SiC epitaxial growth: A comparison with conventional (001) Si substrate," *J. Mater. Res.* **28**, 94–103 (2013).
- ⁵⁴M. Zimbone, M. Zielinski, C. Bongiorno, C. Calabretta, R. Anzalone, S. Scalese, G. Fisicaro, A. La Magna, F. Mancarella, and F. La Via, "3C-SiC growth on inverted silicon pyramids patterned substrate," *Materials* **12**, 3407 (2019).
- ⁵⁵R. Erni, *Aberration-Corrected Imaging in Transmission Electron Microscopy: An Introduction* (Imperial College Press, London, 2010) pp. 1–335.
- ⁵⁶J. Eriksson, M. H. Weng, F. Roccaforte, F. Giannazzo, S. Leone, and V. Raineri, "Toward an ideal Schottky barrier on 3C-SiC," *Appl. Phys. Lett.* **95**, 081907 (2009).
- ⁵⁷J. Eriksson, F. Roccaforte, F. Giannazzo, R. Lo Nigro, V. Raineri, J. Lorenzzi, and G. Ferro, "Improved Ni/3C-SiC contacts by effective contact area and conductivity increases at the nanoscale," *Appl. Phys. Lett.* **94**, 112104 (2009).
- ⁵⁸F. Giannazzo, G. Greco, S. Di Franco, P. Fiorenza, I. Deretzis, A. La Magna, C. Bongiorno, M. Zimbone, F. La Via, M. Zielinski, and F. Roccaforte, "Impact of stacking faults and domain boundaries on the electronic transport in cubic silicon carbide probed by conductive atomic force microscopy," *Adv. Electron. Mater.* **6**, 1901171 (2020).
- ⁵⁹S. Lilov, "Study of the equilibrium processes in the gas phase during silicon carbide sublimation," *Mater. Sci. Eng. B* **21**, 65–69 (1993).
- ⁶⁰W. S. Yoo and H. Matsunami, "Solid-state phase transformation in cubic silicon carbide," *Jpn. J. Appl. Phys.* **30**, 545–553 (1991).
- ⁶¹H. Matsunami and T. Kimoto, "Step-controlled epitaxial growth of SiC: High-quality homoepitaxy," *Mater. Sci. Eng. R* **20**, 125–166 (1997).
- ⁶²R. Püsche, M. Hundhausen, L. Ley, K. Semmelroth, F. Schmid, G. Pensl, and H. Nagasawa, "Study of the temperature induced polytype conversion in cubic CVD SiC by Raman spectroscopy," *Mater. Sci. Forum* **457–460**, 617–620 (2004).
- ⁶³M. Portail, M. Zielinski, T. Chassagne, S. Roy, and M. Nemoz, "Comparative study of the role of the nucleation stage on the final crystalline quality of (111) and (100) silicon carbide films deposited on silicon substrates," *J. Appl. Phys.* **105**, 083505 (2009).
- ⁶⁴D. Rankl, V. Jokubavicius, M. Syväjärvi, and P. Wellmann, "Quantitative study of the role of supersaturation during sublimation growth on the yield of 50 mm 3C-SiC," *Mater. Sci. Forum* **821–823**, 77–80 (2015).
- ⁶⁵S. Datta, *Electronic Transport in Mesoscopic Systems* (Cambridge University Press, 1997).
- ⁶⁶I. Deretzis, M. Camarda, F. La Via, and A. La Magna, "Electron backscattering from stacking faults in SiC by means of ab initio quantum transport calculations," *Phys. Rev. B* **85**, 235310 (2012).
- ⁶⁷J. M. Soler, E. Artacho, J. D. Gale, A. García, J. Junquera, P. Ordejón, and D. Sánchez-Portal, "The SIESTA method for ab initio order-N materials simulation," *J. Phys.: Condens. Matter* **14**, 2745 (2002).
- ⁶⁸J. P. Perdew and A. Zunger, "Self-interaction correction to density-functional approximations for many-electron systems," *Phys. Rev. B* **23**, 5048 (1981).
- ⁶⁹N. Troullier and J. L. Martins, "Efficient pseudopotentials for plane-wave calculations," *Phys. Review B* **43**, 1993 (1991).
- ⁷⁰A. Pimpinelli and J. Villain, *Physics of Crystal Growth, Collection Alea-Saclay: Monographs and Texts in Statistical Physics* (Cambridge University Press, 1998).
- ⁷¹E. Scalise, A. Marzegalli, F. Montalenti, and L. Miglio, "Temperature-dependent stability of polytypes and stacking faults in SiC: Reconciling theory and experiments," *Phys. Rev. Appl.* **12**, 021002 (2019).
- ⁷²D. Hull and D. Bacon, eds., *Introduction to Dislocations*, 5th ed. (Butterworth-Heinemann, Oxford, 2011) pp. 1–257.